Supporting Information

1. Device fabrication

Graphene/hexagonal boron-nitride (hBN) heterostructures were assembled using the dry peel technique[1,2]. To this end, graphite and bulk hBN crystals were first mechanically exfoliated onto an oxidized Si wafer. Monolayer graphene and thin (~30 nm) hBN flakes were then identified by optical microscopy. The flakes were assembled using a polymer membrane attached to the tip of a micromanipulator, which was used as a 'stamp' to pick up and place down the selected crystals. During their assembly, a rotating stage was employed to align crystallographic axes of graphene and the bottom hBN crystal. Because the bulk crystals cleave preferentially along their crystallographic axes, the edges are usually clear and straight, enabling alignment with accuracy of about 0.5^{o}. The resulting alignment produces a moiré potential with a period of about 14 nm[3].

The heterostructures were then made into multiterminal devices such as shown in Fig. S1using electron beam lithography and plasma etching. As the first step, a PMMA mask was fabricated to define long contact regions leading to the heterostructure. Reactive ion etching was then employed to mill through the mask, which produced trenches in the graphene/hBN heterostructure. The same PMMA mask was subsequently used to deposit metal leads into the trenches (3 nm Cr/80 nm Au) which formed quasi-one dimensional contacts to graphene's edges[4,5]. This sequence of steps mitigates the need for graphene to be in contact with any polymer, preserving its high electronic quality. The PMMA mask was removed and a second round of lithography was carried out to define the mesa. Figure S1 shows an example of one of our Hall bar devices. The width of our samples ranged between 1 and 3 μm, and the distance between nearest voltage contacts was at least one width.

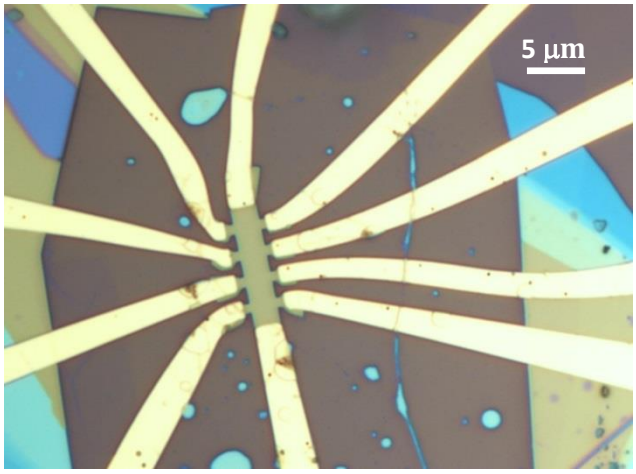

Fig. S1| Graphene/hBN devices. An optical image of one of our superlattice devices. The width of the Hall bar is 3 μm.

www.pnas.org/cgi/doi/10.1073/pnas.1804572115

2. Light doping of graphene/hBN heterostructures

The first order magnetic Bloch states, which are responsible for so-called Brown Zak oscillations, are robust over a wide range of temperatures (T) and carrier density (n). In contrast, even for n close to the secondary Dirac points (DPs), there are no signs of high-order states (p = 2, 3 etc.). To unveil those additional fractal states, we had to dope graphene to much higher n, close to and even beyond $n = 2n_0$ (Fig. 2 of the main text), where n_0 is the carrier density at which secondary DPs occur. To achieve such high n-type doping, we used light illumination as previously reported[6]. In brief, electron donor-like impurity states in hBN are excited by illumination. This leads to positively charged defects that act to dope the graphene sheet negatively. This may happen in both top and bottom hBN layers of our encapsulated devices. Because the defects in hBN are spatially isolated from the graphene channel, the doping has relatively little influence on mobility of charge carriers in the devices. The light-doping effect is sufficiently strong such that we were able to n-dope graphene by $n = 2.5 \times 10^{12}$ cm^{-2} simply using an incandescent light source. Fig. S2 shows the electric-field behavior of our graphene/hBN superlattice devices before and after illumination. Before illumination, the main Dirac point (DP) is found around the applied gate voltage V_G = - 1 V, whereas the secondary DPs are at $\pm$ 15 V. After illumination, the main DP shifted to -20 V, the electron secondary DP to -4 V and the hole secondary DP could not be reached by the electric field doping. Despite this large photo-induced doping, the electronic quality remained high with relatively small degradation in mobility. This is evident from the inset of Fig. S2 which plots the resistivity ρ_{xx} as a function of $V_G - V_{DP}$. Aside from the slight broadening of the main Dirac point after illumination, the curves closely follow each other, in agreement with the previous work[6].

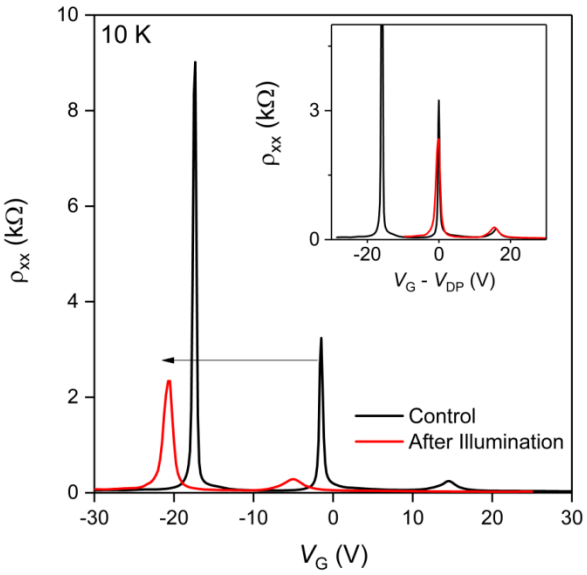

Fig. S2| Light doping of graphene/hBN heterostructures. Longitudinal resistivity ρ_{xx} as a function of gate voltage V_G for one of our graphene devices presented in the main text. Two curves are plotted; before (black curve) and after (red) illumination with an incandescent light source. The black arrow traces the shift in position of the main Dirac point after illumination. Inset; The same data plotted as a function of $V_G - V_{DP}$, where V_{DP} is the position of the main Dirac point.

3. Magnetic mini-bands

Here we describe the model used to calculate the Hofstadter butterfly spectrum and magnetic mini-band structures shown in Figs. 4a-b of the main text. To this end, we consider the electronic spectrum of pristine graphene modified by an underlying moiré potential which is produced by alignment with the hBN substrate. The moiré potential is described by a hexagonal Bravais lattice $n_1\vec{a}_1 + n_2\vec{a}_2$ with a period of the superlattice $a_1 = a_2$. The computed spectrum was obtained using a phenomenological model developed in Ref. 7, which is based on the Hamiltonian.

$$\hat{H} = v_F\vec{p}\cdot\vec{\sigma} + u_0^+ f_+ + \xi\sigma_3 u_3^+ f_- + \frac{\xi}{b}u_1^+\vec{\sigma}\cdot[\vec{\ell}_z\times\nabla f_-],$$

$$f_\pm = \sum\nolimits_{m=1\ldots6}(\pm1)^{m+\frac{1}{2}}e^{i\vec{b}_m\cdot\vec{r}} \quad ,$$

where σ_i are the Pauli matrices acting on the sublattice Bloch states $(\phi_{\mathrm{AK}}, \phi_{\mathrm{BK}})^T$ in the K valley ($\xi = 1$) and $(\phi_{\mathrm{BK'}}, -\phi_{\mathrm{AK'}})^T$ in the K' valley ($\xi = -1$). $f_\pm$ are the six shortest moiré Bragg vectors $\vec{b}_m$ ($b_{1,2,3,4,5,6} = b = \frac{4\pi}{\sqrt{3}a}$) of the superlattice, and u_0, u_1 u_3 are phenomenological parameters' which control the strength of the potential. In our calculations we used $u_0^+ = 21.7$meV, $u_1^+ = -30.6$ meV and $u_3^+ = -22.2$ meV, which is based on previous works that predict the superlattice strength is related to the alignment angle and lattice mismatch of the graphene/hBN lattices (Ref. 7).

In the presence of magnetic field, the Dirac term is modified by the vector potential $\vec{A} = \frac{Bx_1}{a\sqrt{3}}(2\vec{a}_2 - \vec{a}_1)$ and incorporated into the momentum as $\vec{p} = -i\hbar\nabla + e\vec{A}$. We note that $\vec{A}$ is expressed in a hexagonal co-ordinate system (x_1, x_2), such that $\vec{r} = x_1\vec{a}_1 + x_2\vec{a}_2$, to reflect the hexagonal symmetry of the moiré potential in graphene/hBN superlattices, with $\vec{a}_1, \vec{a}_2$ being the basis vectors of the Bravais lattice of the moiré pattern. Without any superlattice, the spectrum consists of infinitely degenerate Landau levels. Mathematically, this is determined by the fact that the group of translations in a magnetic field is non-Abelian[8], since the Aharonov-Bohm[9] effect introduces additional phase factors into the electronic wave function. In the case of the moiré superlattice, for magnetic field $B = \phi_0/S$ (p/q), the Aharonov-Bohm phase attains quantized values of 2π, and the electronic spectrum can then be described by Wannier states which propagate on a supercell that is q times larger than the moiré unit cell (referred to as magnetic Bloch states in the main text). For the analysis of such states, we use the Landau levels to construct a basis set of Bloch-like states. This is done for each point in the miniature Brillouin zone of the corresponding supercell. We then diagonalize the Hamiltonian $\hat{H}$ numerically in that basis, checking the results for convergence against increasing the basis size. The details of such computations and examples of the resulting magnetic miniband spectra can be found in Refs. 7, 10 & 11.

4. Electron transport in the magnetic-minibands

For $\phi/\phi_0 = p/q$, the electrons propagate as if they are in effectively zero magnetic field with a velocity that is determined by details of their magnetic miniband structures (Fig. 4b). This behavior causes local maxima in σ_{xx} to appear at $\phi/\phi_0 = p/q$, with an amplitude that is governed by the Einstein conductivity formula (see Supplementary Information in Ref. 12)

$$\sigma_{xx} = \frac{4e^2}{h}\frac{E_F\tau}{\hbar}\frac{\langle v^2\rangle}{v_F 2} \quad \text{(S2)}$$

where τ is the scattering time, v_F is the Fermi-velocity of graphene, and v is the group velocity of carriers at the Fermi-energy (E_F) in a particular magnetic Bloch state. We note that temperatures T = 100 – 200 K are not insignificant if compared with the width of magnetic-minibands (Fig. 4b), such that thermal smearing could populate carriers with a markedly different velocity to those at the Fermi-energy. Therefore, we consider v averaged over an interval of $\pm k_B T$ around the Fermi-energy, which enters equation (S2) as the mean-square velocity $\langle v^2 \rangle$. Assuming τ is constant[13], $\langle v^2 \rangle$ is the only variable that changes with magnetic field due to the varying miniband structures of magnetic Bloch states that form at different B. We expect the relative amplitudes of local maxima correlate directly with the changes in $\langle v^2 \rangle$ expected for different magnetic Bloch states. We extracted $\langle v^2 \rangle$ by calculating the group velocity for all E within $\pm k_B T$ of E_F and taking the average. The group velocity at each E was determined by the familiar expression

$$\vec{v} = \frac{1}{\hbar}\frac{\partial E(k)}{\partial \vec{k}} \quad \text{(S3).}$$

We calculated $\langle v^2 \rangle$ along a number of arbitrary directions and found the values differed only by about 1 %, which simply reflects a numerical error determined by the discrete set of points in the miniature Brillouin zones used in our simulations.

5. Hierarchy of magnetic Bloch states in the valence band

In the main text, we discussed the visibility of magnetic Bloch states in the conduction band, with regard to transport experiments. In general, we found that magnetic Bloch states with larger p had a smaller group velocity (Fig. 4c of main text). This results in smaller amplitude of σ_{xx} (Fig. 2 of the main text). In experiment, the same qualitative trend was found for hole doping (Fig. 2d). For completeness, we calculated $\langle v^2 \rangle$ for magnetic Bloch states in the valence band at various $\phi/\phi_0 = p/q$ for a given n (Fig. S3). We found the same qualitative trend such that high-order states (larger p indicated by red and blue symbols in Fig. S3) have a systematically smaller $\langle v^2 \rangle$ as compared to the first-order states (black spheres). This demonstrates that the apparent hierarchy of states has a universal behavior for all kind of doping in the graphene/hBN spectrum.

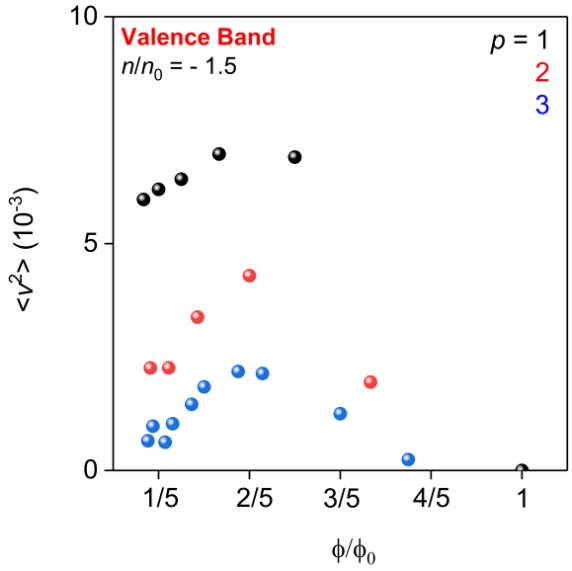

Fig. S3| Group velocity of holes in magnetic minibands. The numerically calculated mean square velocity $\langle v^2 \rangle$ as a function of ϕ/ϕ_0 for different p. Here, we used moiré superlattice parameters listed in Section 3. The black, red and blue symbols correspond to magnetic states with p = 1, 2 and 3 respectively.

References

1. Mayorov, A. S. *et al.* Micrometer-Scale Ballistic Transport in Encapsulated Graphene at Room Temperature. *Nano Lett.* **11,** 2396–2399 (2011).
2. Kretinin, A. V *et al.* Electronic Properties of Graphene Encapsulated with Different Two-Dimensional Atomic Crystals. *Nano Lett.* **14,** 3270–3276 (2014).
3. Yankowitz, M. *et al.* Emergence of superlattice Dirac points in graphene on hexagonal boron nitride. *Nat Phys* **8,** 382–386 (2012).
4. Wang, L. *et al.* One-Dimensional Electrical Contact to a Two-Dimensional Material. *Science* **342,** 614 LP-617 (2013).
5. Ben Shalom, M. *et al.* Quantum oscillations of the critical current and high-field superconducting proximity in ballistic graphene. *Nat. Phys.* **12,** 318 (2015).
6. JuL. *et al.* Photoinduced doping in heterostructures of graphene and boron nitride. *Nat Nano* **9,** 348–352 (2014).
7. Wallbank, J. R., Patel, A. A., Mucha-Kruczyński, M., Geim, A. K. & Fal'ko, V. I. Generic miniband structure of graphene on a hexagonal substrate. *Phys. Rev. B* **87,** 245408 (2013).
8. Wannier, G. H. & Fredkin, D. R. Decoupling of Bloch Bands in the Presence of Homogeneous Fields. *Phys. Rev.* **125,** 1910–1915 (1962).
9. Aharonov, Y. & Bohm, D. Significance of Electromagnetic Potentials in the Quantum Theory. *Phys. Rev.* **115,** 485–491 (1959).
10. Chen, X. *et al.* Dirac edges of fractal magnetic minibands in graphene with hexagonal moire superlattices. *Phys. Rev. B* **89,** 75401 (2014).
11. Chen, X., Wallbank, J. R., Mucha-Kruczyński, M., McCann, E. & Fal'ko, V. I. Zero-energy modes and valley asymmetry in the Hofstadter spectrum of bilayer graphene van der Waals heterostructures with hBN. *Phys. Rev. B* **94,** 45442 (2016).
12. Krishna Kumar, R. *et al.* High-temperature quantum oscillations caused by recurring Bloch states in graphene superlattices. *Science.* **357,** 181 LP-184 (2017).
13. Beenakker, C. W. J. & van Houten, H. Quantum Transport in Semiconductor Nanostructures. in *Semiconductor Heterostructures and Nanostructures* (eds. Ehrenreich, H. & Turnbull, D. B. T.-S. S. P.) **44,** 1–228 (Academic Press, 1991).